Preindustrial to present-day changes in atmospheric carbon monoxide: agreements and gaps between ice archives and global model reconstructions

5 Xavier Faïn[1], Sophie Szopa[2], Vaishali Naïk[3], Patricia Martinerie[1], David M. Etheridge[4,5], Rachael H. Rhodes[6], Cathy M. Trudinger[4,5], Vasilii V. Petrenko[7], Kévin Fourteau[8], Philip Place[7,a]

[1] Univ. Grenoble Alpes, CNRS, INRAE, IRD, Grenoble INP, IGE, 38000 Grenoble, France
[2] Laboratoire des Sciences du Climat et de l'Environnement, CEA, CNRS, UVSQ, Université Paris-Saclay, Gif-sur-
10 Yvette, France
[3] NOAA Geophysical Fluid Dynamics Laboratory, Princeton, NJ, USA
[4] CSIRO Environment, Aspendale, Victoria, Australia
[5] Australian Antarctic Program Partnership, Institute for Marine and Antarctic Studies, University of Tasmania, Hobart, Tasmania, Australia
15 [6] Department of Earth Sciences, University of Cambridge, Cambridge, CB2 3EQ, UK
[7] Department of Earth and Environmental Sciences, University of Rochester, Rochester, NY 14627, USA
[8] Univ. Grenoble Alpes, Université de Toulouse, Météo-France, CNRS, CNRM, Centre d'Études de la Neige, Grenoble, France
[a]: present address: University Instrumentation Center, University of New Hampshire, Durham, NH, 03824, USA
20

Correspondence to: Xavier Faïn (xavier.fain@univ-grenoble-alpes.fr)

Abstract. Global chemistry-climate models (CCMs) play an important role in assessing the climate and air pollution
25 implications of aerosols and chemically reactive gases. Evaluating these models under past conditions and constraining historical sources and sinks necessitates reliable records of atmospheric mixing ratios spanning preindustrial times. Such precious records were recently obtained for carbon monoxide (CO) documenting for the first time the evolution of this reactive compound over the industrial era. In this study, we compare the simulated atmospheric surface CO mixing ratios ([CO]) from two different sets of Climate-Chemistry models and emissions in
30 the frame of CMIP5 and of CMIP6 (Coupled Model Intercomparison Project Phases 5 and 6) with recent bipolar ice archive reconstructions for the period spanning 1850 to present. We analyze how historical (1850-2014) [CO] outputs from 16 ACCMIP (Atmospheric Chemistry and Climate Model Intercomparison Project) models and 7 AerChemMIP (Aerosol Chemistry Model Intercomparison Project) models over Greenland and Antarctica are able to capture both absolute values and trends recorded in multi-site ice archives. While most models underestimate [CO] at high northern
35 latitudes, a reduction in this bias is observed from ACCMIP to AerChemMIP exercises. Over the 1980-2010 CE period, trends in ice archive and firn air observations and AerChemMIP outputs align remarkably well at high northern and southern latitudes, indicating improved quantification of CO anthropogenic emissions and the main CO sink (OH oxidation) compared to ACCMIP. From 1850 to 1980 CE, AerChemMIP models and observations consistently show increasing [CO] in both the Northern Hemisphere (NH) and Southern Hemisphere (SH), suggesting a robust
40 understanding of the CO budget evolution. However, a divergence in the [CO] growth rate emerges in NH between models and observations over the 1920-1980 CE period, attributed to uncertainties in CO emission factors (EF),

particularly EF for RCO (Residential, Commercial and Others) and transportation sectors, although we cannot totally rule out that the CO record based on Greenland ice archives may be biased high by CO chemical production processes occurring in the ice prior the measurements (i.e., in situ CO production). In the Southern Hemisphere, AerChemMIP

45   models simulate an increase in atmospheric [CO] from 1850 to 1980 CE closely reproducing the observations (22±10 ppb and 13±7 ppb, respectively). Such agreement supports CMIP6 biomass burning CO emission inventories which do not reveal a peak in CO emissions in the late 19th century. Furthermore, both SH models and observations reveal an accelerated growth rate in [CO] during 1945-1980 CE relative to 1850-1945 CE, likely linked to increased anthropogenic transportation emissions.

50   **1 Introduction**

Carbon monoxide (CO) is an air pollutant that affects the oxidizing capacity of the troposphere and contributes to ozone formation (Crutzen, 1973). Its primary loss is through reaction with OH with a small contribution from dry deposition, which leads to an atmospheric lifetime of about 2 months (Khalil et al., 1999). Thus, CO is an excellent tracer of long-range transport and an integrator of atmospheric chemical processes. In the modern atmosphere, the

55   main sources of CO are combustion (fossil fuel and biomass burning) and secondary production in the atmosphere (atmospheric oxidation of methane (CH_4) and non-methane volatile organic compounds (VOCs)). Methane oxidation currently amounts to 70-80 % of the secondary atmospheric CO production (Duncan et al., 2007; Fortems-Cheiney et al., 2012). CO surface emissions include biomass burning (van der Werf et al., 2017), incomplete combustion of anthropogenic fossil fuels and biofuels (Hoesly et al., 2018), and minor contributions from the ocean (Conte et al.,

60   2019) and plant leaves (Bruhn et al., 2013). Incomplete fossil fuel combustion represents ~70% of CO primary emissions (Szopa et al., 2021, and references therein). A schematic overview of the modern global CO budget is given in Fig. 1.
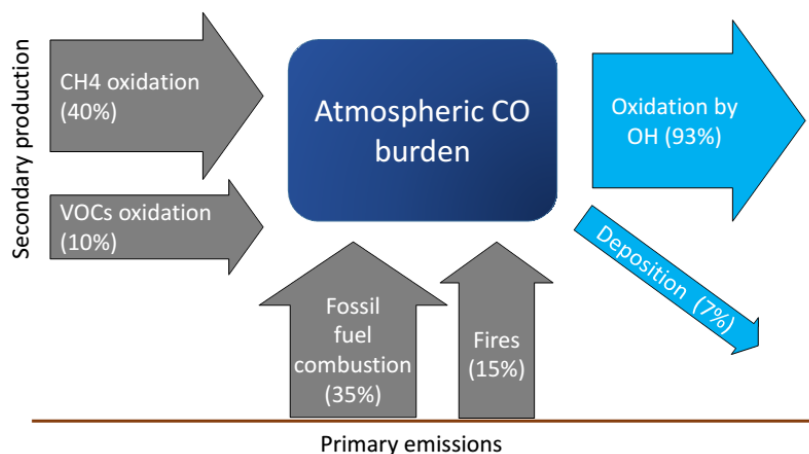
Figure 1. Modern budget of atmospheric CO. Primary emissions and secondary production each amount to ~50% of CO
65   **sources (Szopa et al., 2021). Primary emissions for plant leaves and oceans are small and not shown here, the proportion of emissions from fossil fuel combustion and fires is 35% and 15%, respectively (Szopa et al., 2021). Secondary CO production is dominated by CH_4 oxidation which amounts to ~35-40% of the global CO source, with VOCs oxidation accounting for ~10-15% (Duncan et al., 2007; Fortems-Cheiney et al., 2012). The main CO sink is through OH oxidation, which accounts for more than 90% of CO removal (Khalil et al., 1999; Stein et al., 2014).**

70 Recent advances in satellite retrievals, ground based column observations, airborne platforms, surface measurement networks and assimilation products have improved the characterization of the present-day atmospheric CO distribution (Szopa et al., 2021, and reference therein). Typical annual mean surface CO concentrations range from ~120 ppb in the Northern Hemisphere (NH) to ~40 ppb in the Southern Hemisphere (SH) (Petron et al., 2023). A study using data assimilation techniques estimates a global mean CO burden of 356 ± 27 Tg over the 2002-2013 period (Gaubert et al.,

75 2017). There is high confidence that global CO burden has been declining since 2000 (Szopa et al., 2021, and references therein), although this global decreasing trend in CO has shown a slowdown over the last 5 years (Buchholz et al., 2021; Petron et al., 2023).

Recent analytical and modeling advances applied to ice archives (firn air and bubbles trapped in deep ice) from both Greenland (Petrenko et al., 2013; Faïn et al., 2022) and Antarctica (Faïn et al., 2023; Strawson et al., 2024) have

80 allowed the production of a new bipolar reconstruction of atmospheric carbon monoxide including preindustrial (PI) times and spanning 1700-1992 CE (resp. 1700-2016) in the SH (resp. in the NH). These reconstructions can be extended to present day using direct measurements of atmospheric [CO] at high latitudes, e.g. at Mawson or South Pole stations (Antarctica) and Cape Grim station (Australia) in the SH (Faïn et al., 2023; Loh et al., 2021).

Estimates of global anthropogenic emissions of both CO and its precursors have been revised recently for use in the

85 Coupled-Model Intercomparison Project 6 (CMIP6) (Collins et al., 2017). Hoesly et al. (2018) have extended these estimates of anthropogenic emissions back to 1750 and developed differentiation (source sector-wise) and gridding of emissions (Feng et al., 2020). Similarly, biomass burning CO emissions, which represent about 30% of present-day global CO emissions (i.e., about 15% of global CO sources, Fig. 1) have been revised in the framework of CMIP6 (van Marle et al., 2017). CMIP6 biomass burning CO emissions, which assume that fires scale up with population

90 density, increase only slightly from 1750 to 2015 CE and peak during the 1990s after which they decrease gradually and consistently. However, fire emissions reaching higher levels in the PI compared to present day have been recently suggested (Hamilton et al., 2018; Liu et al., 2021; Rowlinson et al., 2020) as a result of a possible decline in burned areas with increasing population density due to land use changes (Andela et al., 2017; Knorr et al., 2014).

CMIP6 updated anthropogenic and biomass burning CO emissions inventories have been used by a set of state-of-

95 the-art global chemistry-climate models (CCMs) to investigate the trends in global tropospheric hydroxyl radical and methane lifetime (Stevenson et al., 2020) and the evolution of the tropospheric ozone burden and budget terms (Griffiths et al., 2021) since 1850 CE. Climate-Chemistry Models (CCMs) suggest that the global CO tropospheric burden has increased by ~120 Tg since 1850 (Fig. 1 in Griffiths et al., 2021), with: (i) a moderate increase rate from 1850 to 1950 CE, (ii) a fast increase rate from 1950 to 1990 CE, and (iii) a decrease trend from 1990 and 2015 which

100 reproduces the observed decline in tropospheric [CO] (Szopa et al., 2021, and reference therein).

In this paper we compare trends in atmospheric surface [CO] simulated by two different sets of CCMs and emissions in the frame of CMIP5 (Lamarque et al., 2013) and of CMIP6 with recent reconstructions from polar ice archives for the period spanning 1850 CE to present. The aim of this work is to establish the periods of robust agreement between models and data, indicating a robust knowledge of trends in emissions and adequate fit-for-purpose of the models over

105 such periods, and discuss the possible reasons for disagreement over specific periods.

2. Bipolar [CO] reconstructions from polar ice archives

Ground based and satellite-derived CO data are only available for the last three decades. Ancient air preserved in glacial ice and firn is thus a unique archive for reconstructing the past atmospheric [CO] record prior to the 1990s. A large amount of air can be sampled from the interconnected open pores of the firn, which is the upper layer of an ice sheet where snow is slowly transformed into ice. Mean ages of atmospheric gases increase with firn depth to about a century ago. Analysis of air trapped in bubbles in solid ice below the firn layer is required to extend reconstructions further back in time, and can now be conducted by Continuous Flow Analyses (CFA) which produce continuous, high resolution, datasets (Faïn et al., 2023, 2022, 2014).

By analyzing [CO] depth profiles collected from firn air at three different Greenland sites (NGRIP, Summit, and NEEM), Petrenko et al. (2013) obtained a reconstruction of atmospheric [CO] spanning 1950-2010 CE. Over the same period, stable isotopes of CO (i.e., $\delta^{13}CO$ and $\delta C^{18}O$) were analyzed in firn air samples collected at the NEEM site to provide additional powerful clues for the interpretation of the changes in the CO budget (Wang et al., 2012). The reconstruction from Petrenko et al. (2013) has been recently extended back to 1700 CE with the CFA analysis of 4 different Greenland ice cores (Fig. 2, upper panel, NGRIP, PLACE, NEEM, and D4) (Faïn et al., 2022). Faïn et al. (2022) could not fully exclude the possibility that the Greenland ice archive CO reconstruction could be slightly positively biased by chemical processes (in situ production) occurring within the Greenland ice. Therefore, the atmospheric [CO] history extracted from Greenland should be considered as an upper bound of the past [CO] in the Arctic (Faïn et al., 2022). The temporal changes depicted by this historical Greenland [CO] record probably have a larger spatial significance than the Arctic context alone, as suggested by the GAW (Global Atmospheric Watch) reactive gases measurement network (Petron et al., 2023; Schultz et al., 2015).

Ice archives from Antarctica were also investigated: CO was collected in firn air at seven sites (Lock In, DE08-2, DSSW19K, DSSW20K, South Pole, ABN, and Berkner Island) to reconstruct [CO] in the Antarctic atmosphere from 1898 CE to present (Fig. 2, lower panel; Faïn et al., 2023). CFA analyses conducted on three ice cores (DC12, ABN, and TaldIce) extended this reconstruction back for three millennia starting 1897 CE (Faïn et al., 2023). Ice core and firn air measurements, as well as firn air and direct atmospheric measurements, show excellent agreements during intervals of overlap. These Antarctic CO records appear to be unaffected by in situ CO production or sampling artifacts, and are in excellent agreement with a recent ice core CO record from the Antarctic Peninsula spanning 1821-1995 CE (Fig. 2; Strawson et al., 2024), although the Peninsula CO record reveals multi-decadal variability due to higher accumulation ice archives. These new Antarctic CO reconstructions suggest that the previously published Antarctic [CO] datasets (Haan et al., 1996; Haan and Raynaud, 1998; Wang et al., 2010) were likely biased high. The [CO] reconstruction based on Antarctic ice archives reported on Fig. 2 is representative of the 45-90°S atmosphere, with temporal changes having probably a larger spatial significance, including at least the 30-90°S latitudinal band (Faïn et al., 2023).
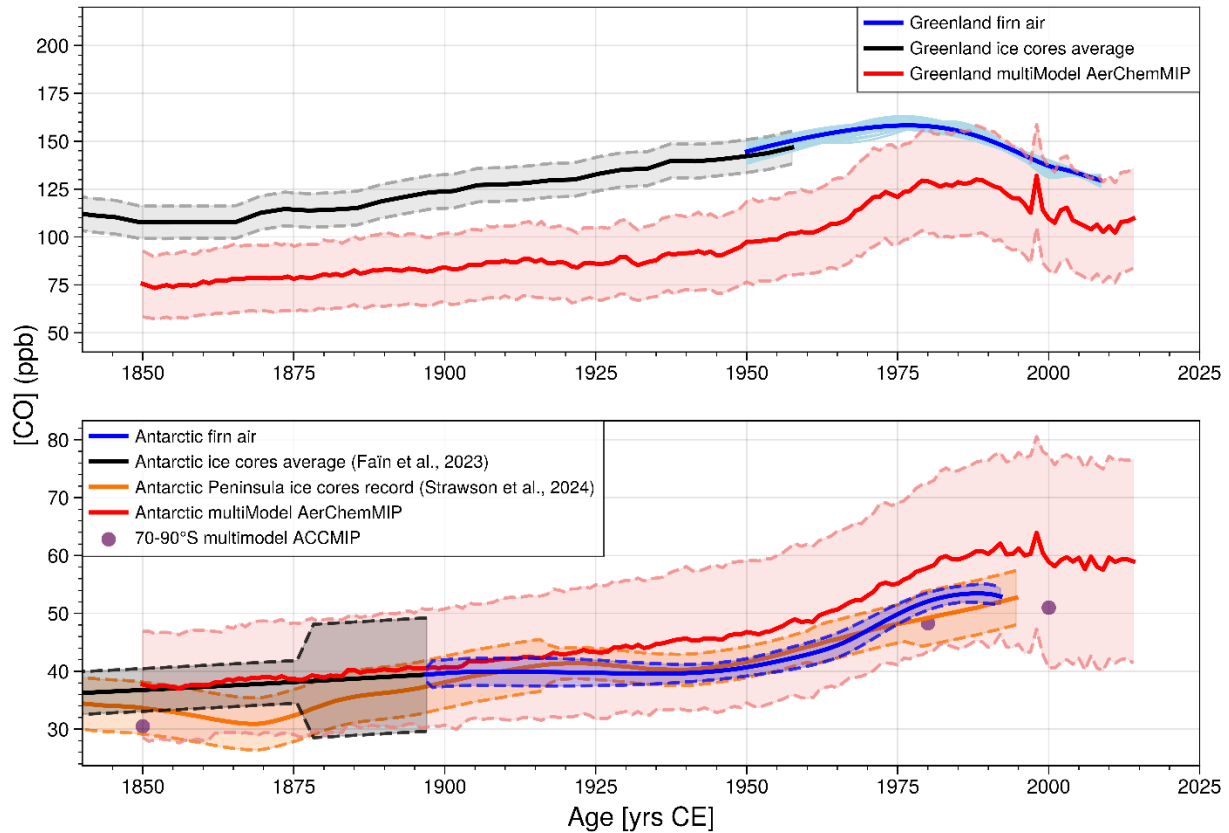
140

Figure 2. Greenland (upper panel) and Antarctic (lower panel) atmospheric [CO] from ice cores and firn air reconstructions (Faïn et al., 2023, 2022; Petrenko et al., 2013); from NOAA and CSIRO atmospheric monitoring; and from Multimodel AerChemMIP historical [CO] simulations (red line). The grey envelope on the Greenland (resp. Antarctica) ice core [CO] record reports 1σ (resp. 2σ) uncertainty (Faïn et al., 2023, 2022). On the upper panel, light blue denotes the firn air records

145 **obtained by combining samples from three Greenland sites and is a metric of the uncertainty, and blue represents the average firn air record (Petrenko et al., 2013). On the lower panel, the blue envelope on the Antarctic firn air [CO] reconstruction reports 2σ uncertainty. The recent CO record from the Antarctic Peninsula (Strawson et al., 2024) is shown in orange with a combined 2σ uncertainty envelope. The red envelopes on the AerChemMIP simulations show 1σ uncertainties. The multimodel ACCMIP [CO] is also reported for 1850, 1980 and 2000.**

150 **3. The ACCMIP exercise**

The Atmospheric Chemistry and Climate Model Intercomparison Project (ACCMIP), which was part of CMIP5, consisted of a series of time slice experiments to investigate long-term changes in atmospheric composition between 1850 and 2100 CE, and how composition changes impact radiative forcing (Lamarque et al., 2013).

5

3.1. ACCMIP CO budget

3.1.1. CO sources

Anthropogenic and biomass burning CO emissions used in the frame of ACCMIP are taken from the RETRO and EDGAR-HYDE inventories (Lamarque et al., 2010). Natural emissions for CO were specified from different sources depending on models.

3.1.2. CO sinks

Sinks for atmospheric CO include oxidation with OH radicals and CO uptake via oxidation by soil microbes. Reaction with OH radicals acts as the major CO sink while deposition in soils contributes about 10% to the global atmospheric CO losses (Duncan et al., 2007; Khalil et al., 1999; Stein et al., 2014). ACCMIP models exhibit a large diversity in the magnitude and sign of PI to present-day OH changes (ranging from a decrease of 12.7% to an increase of 14.6 %). Despite large regional changes, the multi-model global mean (mass-weighted) OH concentration changes little over the past 150 yrs (Naik et al., 2013). For the 1980 to 2000 period, ACCMIP models find a slight increase in mean OH (3.5 ± 2.2 %) (Naik et al., 2013).

3.2. Model outputs

In this study, we extract historical CO mixing ratio outputs from the 16 ACCMIP models (Naik et al., 2013) available at the CEDA dataset repository (https://catalogue.ceda.ac.uk/) for three time slices (1850, 1980, and 2000 CE) over two areas (i) Greenland (60-20°W; 84-60°N), and (ii) Antarctica (90-70°S). For each time slice, a single mutlimodel mean [CO] is obtained by averaging CO outputs of the 16 models. Figure 2 (resp. Fig. 3) reports the ACCMIP multimodel CO absolute levels (resp. the anomaly relative to the 2000 CE) for both Arctic and Antarctic atmospheres (in ppb).
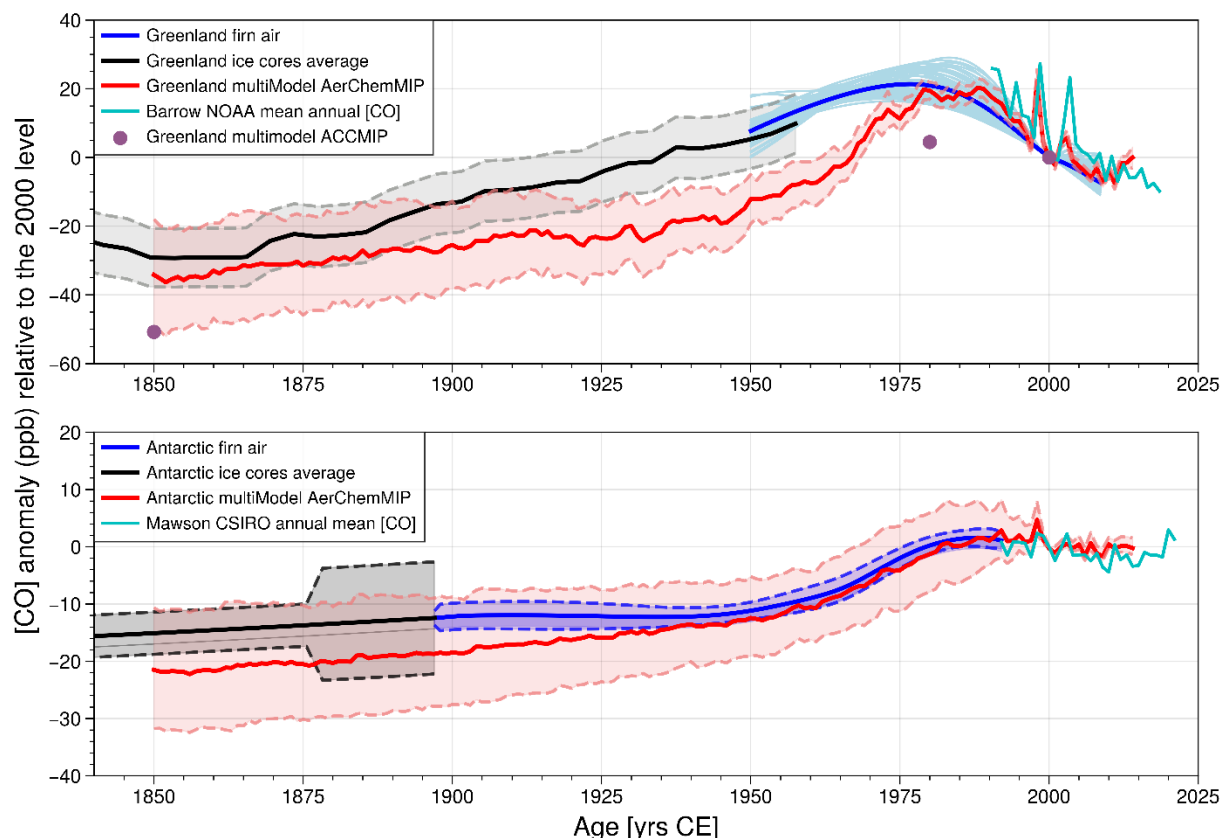
Figure 3. Anomaly of Greenland (upper panel) and Antarctic (lower panel) atmospheric [CO] from ice cores and firn air reconstructions (Faïn et al., 2023, 2022; Petrenko et al., 2013); from NOAA and CSIRO atmospheric monitoring; and from Multimodel AerChemMIP historical simulations (red line). The grey envelope on the Greenland (resp. Antarctica) ice core [CO] record reports 1σ (resp. 2σ) uncertainty (Faïn et al., 2023, 2022). On the upper panel, light blue denotes the firn air records obtained by combining samples from three Greenland sites and is a metric of the uncertainty, and blue represents the average firn air record (Petrenko et al., 2013). On the lower panel, the blue envelope on the Antarctic firn air [CO] reconstruction reports 2σ uncertainty. The red envelopes on the multimodel AerChemMIP simulations show 1σ uncertainties. The multimodel ACCMIP [CO] anomaly is also reported for 1850, 1980 and 2000. All data are reported as anomalies relative to annually-averaged 2000 levels.

4. The AerChemMIP exercise

The Aerosol Chemistry Model Intercomparison Project (AerChemMIP) is part of CMIP6 and aims to quantify the climate and air quality impacts of aerosols and chemically reactive gases, including CO (Collins et al., 2017). In this study, we use the historical (1850-2014) CO mixing ratios outputs from seven models involved in the AerChemMIP exercise: UKESM1-0-LL (Archibald et al., 2020), GFDL-ESM4 (Dunne et al., 2020; Horowitz et al., 2020), CESM2-WACCM (Emmons et al., 2020), BCC-ESM1 (Zhang et al., 2021; Wu et al., 2020), GISS-E2 (Bauer et al., 2020), MRI-ESM2 (Yukimoto et al., 2019) and EC-Earth3 (van Noije et al., 2021). No criteria were applied to select specific models, and we included in this study all CO modeling results available on the ESGF datasets repository at the end of July 2024.

4.1. AerChemMIP CO budget

4.1.1. CO sources

Anthropogenic and biomass burning CO emissions used in the framework of AerChemMIP have recently been produced specifically for CMIP6 for the 1750-2014 CE period, and are common to all models. Anthropogenic CO emissions are reported by Hoesly et al. (2018) and include aircraft, energy production, industry, residential commercial and others, shipping, transportation on land, and waste (including waste burning). Biomass burning CO emissions are based on merging satellite observations with proxies and fire models (van Marle et al., 2017).

Biogenic sources are not constrained by the AerChemMIP protocol. Biogenic VOC (BVOC) emissions are often interactive: CESM2, GFDL and BCC models use the same emission model (MEGAN, Guenther et al., 2006), while UKESM1 or GISS-E2 apply different models (Pacifico et al., 2011, and Shindell et al., 2006, respectively). MRI-ESM2 and EC-Earth3 models prescribe constant BVOC emissions (Oshima et al., 2020; van Noije et al., 2021). A comparison of BVOC emissions for five of the models involved in this study is provided by Griffiths et al., (2021, Fig. 1). The direct CO emission from biogenic sources (e.g., plant leaves) is low, but the emissions of biogenic VOCs (BVOCs), later oxidized into CO, is a large source of atmospheric CO (Fig. 1).

For all models, CH_4 mixing ratios are prescribed at ground levels using ice core reconstructions (Meinshausen et al., 2017). CH_4-oxidation CO source is thus well constrained in terms of trend but can vary accordingly to absolute OH values differing from one model to another.

4.1.2. CO sinks

AerChemMIP models simulate stable global OH from 1850 to 1980, and a 10% increase in global OH since 1980, indicating that no changes in the major CO sink are modeled prior to 1980 (Stevenson et al., 2020). However, spatial distribution of the OH radical, which differs among models (Stevenson et al., 2020), can have a large impact on the main CO sink (Strode et al., 2015).

Although much smaller, the CO sink driven by dry deposition into soils is included in the AerChemMIP models (e.g., Archibald et al., 2020; Emmons et al., 2020; Horowitz et al., 2020). However, this CO sink remains poorly constrained as little focus has been placed so far on the role of CO dry deposition in global modeling (Stein et al., 2014).

4.2. Model outputs

In this study, we extract historical (1850-2014) CO mixing ratio outputs from the 7 AerChemMIP models mentioned earlier over the same two areas already defined for ACCMIP simulation (Sect 3.2): (i) Greenland (60-20°W; 84-60°N), and (ii) Antarctica (90-70°S). For each model, we first obtain a single time series by averaging all members available on the ESGF datasets repository (https://aims2.llnl.gov/search) at the end of July 2024. For each area (Greenland and Antarctica), model outputs are thus combined to produce (i) a multimodel history of absolute [CO] (Fig. 2, red line), and (ii) a multimodel [CO] trend defined as [CO] anomaly relative to the 2000 CE [CO] level (Fig. 3, red line). The envelopes reported on Fig. 2 and 3 (1-σ) represent the variability in simulated [CO] among the 7 models and can be interpreted as the uncertainty in how state-of-the-art CCMs can simulate historical [CO]. Individual model outputs are reported on Fig. S1 (Greenland) and Fig. S2 (Antarctica). Interestingly, while differences in transport dynamics and

235   chemical schemes (e.g., Shindell et al., 2006) drive a wide range of CO burdens among models, they do not drive a large diversity in modeled trends (Fig. S1 and S2). One of the 7 models, the BCC-ESM1 model, exhibits a larger CO burden, but excluding this "outlier" model has little effect on the multimodel mean results.

5. New insights into past CO budget

In this section, we compare observations (i.e., historical reconstructions retrieved from ice archives, Sect. 2) with
240   ACCMIP and AerChemMIP multimodel outputs (Sect. 3 and 4), at both high northern and southern latitudes, to infer new constraints on past CO sources and sinks.

5.1. Model bias of [CO] at high latitudes

We observe discrepancies in absolute [CO] values between model output and ice archive datasets (Fig. 2). AerChemMIP model mean is about 20% lower than ice archive datasets at high northern latitudes along the entire
245   1850-2014 period. At high southern latitudes, AerChemMIP model mean is in good agreement with ice archive dataset during the period spanning 1850-1900, with a positive bias slowly increasing from 1900 to 1970, to reach modeled [CO] about 20% higher than ice core archives during the last three decades. Such discrepancies also exist for the recent two decades with surface ground observations (e.g., at Barrow, Alaska, USA and Mawson, Antarctica, Fig. 2). However, AerChemMIP model mean agrees with the ice core record at Antarctica within its 1-σ variability envelope,
250   and we thus focus here on the NH [CO] model bias.

Negative bias in the AerChemMIP model mean [CO] at northern mid to high latitudes (Fig. 2) is consistent with systematic underestimation of observed [CO] at these latitudes, but the hypotheses to explain such bias vary between studies. Missing anthropogenic emissions from the inventories are commonly hypothesized to explain the negative CO bias (e.g., Emmons et al., 2020; Heimann et al., 2020; Miyazaki et al., 2020; Shindell et al., 2006; Stein et al.,
255   2014). However, underestimation of the secondary CO production from chemical oxidation of methane or VOCs could also be involved (e.g., Archibald et al., 2020; Gaubert et al., 2017; Heimann et al., 2020), as well as CO losses via OH oxidation (Archibald et al., 2020; Strode et al., 2015) or soil deposition (Stein et al., 2014). Recent studies have suggested mitigating the negative CO bias in the NH by assimilating multiple datasets of chemical observations (e.g., Gaubert et al., 2020; Miyazaki et al., 2020; Zheng et al., 2019). The causes of CO negative biases at northern mid to
260   high latitudes in CCMs remain highly debated, but targeted sensitivity experiments for bias attribution are outside the scope of this study. However, how models represent absolute [CO] at northern latitudes has improved over the last decade, as shown by the reduction in negative bias in model mean [CO] between the ACCMIP and the AreChemMIP exercises (Fig. 2). Furthermore, not all models exhibit a negative bias at high northern latitudes, for e.g. the UKESM1 model accurately simulates the absolute [CO] observed at Barrow (AK) over the last 3 decades, or the BCC-ESM1
265   model shows a positive bias (Fig. S1).

5.2. Global decline in atmospheric [CO] since 1990 CE

Over the period spanning 1990-2010 CE, trends in observations and AerChemMIP multimodel outputs are in excellent agreement at both northern and southern high latitudes (Fig. 3). Trends in atmospheric [CO] are defined here as

variations in [CO] relative to the year 2000 CE. In the SH, [CO] trend observed at Mawson station (-0.15±0.04 ppb yr^{-1}, 1σ, p<0.01) agrees within its uncertainty range with [CO] AerChemMIP multimodel trend (-0.20±0.07 ppb yr^{-1}, 1σ, p<0.01). In the NH, [CO] trends are almost identical between atmospheric monitoring (Barrow, -1.27±0.16 ppb yr^{-1}, 1σ, p<0.01), Greenland firn air reconstruction (-1.14±0.01 ppb yr^{-1}, 1σ, p<0.01) and models (-1.22 ±0.16 ppb yr^{-1}, 1σ, p<0.01) during the 1990-2010 CE period. Isotopic CO analysis conducted on Greenland firn air suggest that the decline in Arctic [CO] between the peak in the 1970s and 2000 is due almost entirely to reduced fossil fuel emissions, specifically reductions from road transportation (Wang et al., 2012). Over the recent decades, AerChemMIP models also successfully capture at different latitudes the amplitude and phase of the [CO] seasonal cycle as well as the magnitude of interannual variability in atmospheric [CO] revealed by direct atmospheric monitoring (Archibald et al., 2020; Emmons et al., 2020; Horowitz et al., 2020). Figure 3 reveals how AerChemMIP models reproduce interannual variability in Arctic [CO], driven by biomass burning (e.g., during summer 1998 CE). Such variability is not captured by ice archives due to the temporal smoothing introduced by gas diffusion in polar firn.

Recent decades are when surface emissions of CO are the best constrained (Hoesly et al., 2018). NMVOCs emissions are also precisely quantified (Hoesly et al., 2018), and atmospheric [CH$_4$] is prescribed using ice core records (Meinshausen et al., 2017), thus CO secondary production is also well known. The good agreement in the trends between model outputs and observations suggest that the main CO sink (OH oxidation) is also accurately represented within models. AerChemMIP models report stable global levels of tropospheric OH from 1850 to 1980 CE, and a ~10% increase in OH from 1980 to 2014 CE (Fig. 2a from Stevenson et al., 2020). The good agreement in the trends between models and observations reported here lends credibility to the OH trend simulated by AerChemMIP models. It also suggests that the recent increase in anthropogenic NOx emission is well understood.

Figure 3 also includes a comparison between AerChemMIP and ACCMIP modeling outputs, with ACCMIP temporal resolution being much more limited. The ACCMIP multi-model simulation of the Arctic [CO] is only 4 ppb lower in 2000 CE compared to 1980 CE (Naik et al., 2013). ACCMIP models were not able to fully reproduce the decline in Arctic [CO] reconstructed for the last decade. Petrenko et al. (2013) already reported a poor agreement between the trends from a firn air [CO] record and a CAM-Chem historical run, which was part of the ACCMIP exercise. One possible reason for such improvement in the framework of AerChemMIP are the anthropogenic emissions, dominant over the last decades, which are better constrained now (Hoesly et al., 2018). Also, modeled trends in secondary CO sources (notably oxidation of VOCs) are difficult to compare across the different generations of models because of the lack of required outputs. Since models vary in their representation of the chemical mechanisms (and therefore VOC chemistry), we expect this to be a driving factor in the diversity of CO trends similar to that for O$_3$ (Young et al., 2013, Griffiths et al., 2021). Additionally, trends in OH, which is the primary sink for CO, also vary across the models (Naik et al. 2013, Stevenson et al., 2020). Analyzing the inter-exercise (ACCMIP vs AerChemMIP) and inter-model (see Sect. 5.1) differences in atmospheric [CO] levels would require more outputs from the models that have not been archived and sometimes extra simulations, and is beyond the scope of this study.

5.3. Increase in Northern Hemisphere atmospheric [CO] from 1850 to 1980 CE

Along the time period spanning 1850-1980 CE, both AerChemMIP models and observations exhibit increasing [CO] (Figs. 2 and 3). At northern latitudes, the increase in [CO] simulated from 1850 to 1980 CE is ~55 ppb, in excellent agreement with observations that reveal a ~50 ppb increase for this period. NH simulated and observed trends in [CO] agree within their 1σ uncertainties prior to 1920 but diverge during the 1920-1980 CE period. While the ice core and firn based record exhibit an increase in [CO] at a steady rate of ~0.5 ppb yr^{-1}, the AerChemMIP multimodel average reveals slow growth from 1920 to 1945 at a rate of ~0.2 ppb yr^{-1}, which quickens from 1945 to 1980 with a rate of ~1.1 ppb yr^{-1}. At southern latitudes, AerChemMIP models simulate a larger increase in atmospheric [CO] from 1850 to 1980 CE than observations (22±10 ppb and 13±7 ppb, respectively), although model outputs and ice archive datasets always agree within their 1σ uncertainties. Both models and observations also reveal an increase in [CO] growth rate in the SH, which is twice as large between 1945 and 1980 CE as it was between 1850 and 1945 CE. Finally, over the time period spanning 1850-1980 CE, the [CO] trends simulated by ACCMIP datasets are similar to those produced in the frame of AerChemMIP (Fig. 3). For this period, a key improvement of AerChemMIP compared to ACCMIP is the annual resolution of the model runs.

The general agreement between simulated and observed [CO] trends, both in the NH and SH, for the period spanning 1850-1980, indicate a good overall understanding of the evolution of the CO budget over this period. However, a mismatch in [CO] trends remains between the AerChemMIP multimodel mean and the ice archive dataset in the NH for the period spanning 1920 to 1980 CE, with the multimodel mean showing a lower trend before 1945, and a higher trend after 1945(Fig. 3). The CO record based on Greenland ice archives should be considered as an upper bound of the past CO abundance, and we cannot fully rule out that in situ production artifact (Faïn et al., 2022) impacting ice and firn air samples explain such mismatch (Sect. 2). However, the Greenland ice archives record is a combination of 5 ice core and 3 firn air records, which all support an increase in [CO] at a steady rate during the 1920-1980 CE period (Faïn et al., 2022). We thus investigate if uncertainties in descriptions of CO sources and sinks used by AerChemMIP models can explain the differences in [CO] growth rate between models and observations for the period spanning 1920-1805 CE.

5.3.1. OH-oxidation CO sink

A first hypothesis to explain the differences in trends between ice archive and model [CO] in the NH for the period spanning 1920-1980 could be an inaccurate estimation of the OH-oxidation CO sink by models. AerChemMIP simulations suggest that global tropospheric hydroxyl radical changes little from 1850 to 1980 CE (Stevenson et al., 2020). Global OH reconstructions are not easily comparable with Greenland [CO] reconstructions because OH is more abundant in the tropics whereas the latitudinal band that is of most importance for polar CO is considerably narrower, likely ~30–90°, because of the relatively short CO atmospheric lifetime. Ozone precursor (NOx, CO, and VOC) emissions have strongly influenced OH trends, specifically the relative roles of changing emissions of CO and NOx have important competing consequences. Higher concentrations of NOx increase OH through ozone photochemical production and the subsequent reaction with H_2O to produce OH, as well as recycling of HO_2 to OH. On the other hand, higher concentrations of CO and VOCs (and CH_4) will reduce OH. Stevenson et al. (2020) report a dominant

role of NOx emission increases, whose impact overwhelms the impacts of increasing CO (up to the 1990s) and VOCs emissions, which will have tended to reduce OH. Finally, the OH-oxidation CO sink modelled in the framework of AerChemMIP is closely related to NOx emission inventories. To reconcile modeled and ice core-based NH CO trends, a decrease in the OH-oxidation CO sink would be required during the period spanning 1870-1945 CE, which would mean lower NOx emissions. The CMIP6 NOx emissions remain low before 1945 CE (Fig. 1 in Stevenson et al., 2020). Considering the period spanning 1945-1980 CE, an increase in the OH-oxidation CO sink would be required to reconcile modeled and observed [CO] growth rates. Overall, if an inaccurate estimation of the OH-oxidation CO sink by models was the cause of the mismatch between observed and modeled NH [CO] trend, it would imply centennial variation in global OH, with unlikely low OH levels in the early 20th century. A diversity of models is involved here (i.e. diversity of chemical schemes) and the drivers of variability in global OH can be very different between models (Wild et al., 2020). However, most CCMS models show buffered OH at global scale (Stevenson et al., 2020), and our comparison between modeled and observed CO record supports this conclusion.

5.3.2. CO secondary production

If we hypothesize that the past evolution of OH levels is well understood for the period spanning 1920-1980 (Stevenson et al., 2020), CO sources should be investigated to explain the mismatch between modeled and observed CO trends over the time period 1920-1980 CE: secondary production and/or direct emissions may be involved. Secondary production represents in the modern atmosphere about 50% of the CO sources (Fig. 1, Szopa et al., 2021), and is largely driven by methane oxidation. CEDS anthropogenic global methane emissions exhibit an 8-fold increase from 1850 to present (Stevenson et al., 2020), but for all AerChemMIP simulations atmospheric CH_4 levels are prescribed at the surface based on observations and ice core data (Meinshausen et al., 2017). Thus atmospheric CH_4 is well constrained, and the CH_4-oxidation CO source is accurately quantified by models. On the other hand, VOCs-oxidation represents only a small fraction of the modern CO sources (~10%, Fig. 1; Fortems-Cheiney et al., 2012). AerChemMIP models suggest no large changes in BVOC emissions for the 1850-1980 CE period (Griffiths et al., 2021). Using the dynamic global vegetation model LPJ-GUESS, Hantson et al. (2017) find that both isoprene and monoterpene, which represent the largest fraction of BVOC, had higher emissions at the beginning of the 20th century than at present. AerChemMIP models suggest an increase in the growth rate of anthropogenic VOCs (AVOCs) emissions in the 1950s (Stevenson et al., 2020). However, AVOC oxidation represents a minor source of CO and an underestimation of the AVOCs emission prior to 1950 CE is unlikely to explain the differences in modeled and ice archive [CO] NH trends (Fig. 3).
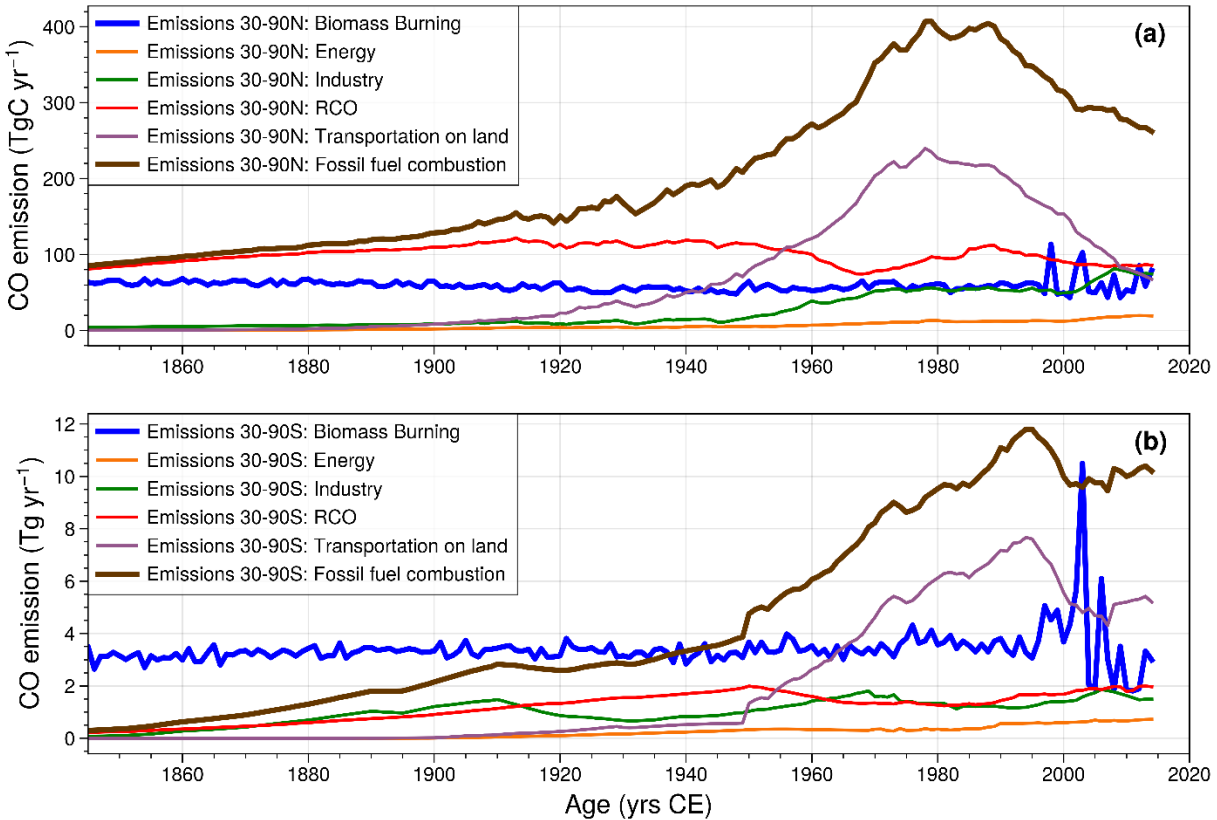
5.3.3. CO anthropogenic emissions

In the period spanning 1850-1980 CE, the multimodel mean of Arctic [CO] (Fig. 3) evolves with a rate similar to that of its direct emissions in the 30-90°N latitudinal band (Fig. 4). This direct emissions rate is driven by change in emissions due to fossil fuel combustion itself driven by changes in emissions from transportation (brown and purple lines on Fig. 4; Hoesly et al., 2018). According to the inventory used in CMIP6, CO biomass burning emissions exhibit little variation since 1850 CE (blue line on Fig. 4; van Marle et al., 2017). Prior to 1945 CE, direct anthropogenic CO

emissions are largely dominated in magnitude by the RCO (residential, commercial, others) sector. In 1945 CE, CO emissions related to transportation started increasing, rapidly dominating other emissions sectors, including RCO (Fig. 4). Combustion of fossil fuels is the driver of the trends in CO_2 emissions over the 20th century (see Fig. 2.1 panel A of the IPCC, 2023 synthesis report). CO_2 atmospheric levels are reconstructed thanks to multiple ice core and firn records and have been directly measured at a growing number of surface stations since 1945. The atmospheric CO_2 record brings a strong constraint on fossil fuel combustion inventories which can be considered as robust. Fossil fuel combustion inventories (also referred as activity dataset) are combined with emission factors (EFs) to estimate atmospheric gaseous emissions. There is a high confidence in emission factors for CO_2 but Hoesly et al. (2018) report that anthropogenic CO EF prior to 1970 are not well constrained. Combustion EF for CO are held constant before 1900 at values drawn from a literature review (Winijkul et al., 2016), and linearly interpolated between 1900 and 1970 by Hoesly et al. (2018). Consequently, we suggest that the mismatch in [CO] trends observed between the AerChemMIP multimodel mean and the ice archive dataset in the NH for the period spanning 1920 to 1980 CE (Fig. 3) may be related to uncertainties in CO EF, specifically EF for the RCO and transportation sectors which drive the direct CO emission pattern during the 1920-1980 CE period.

Figure 4. CEDS anthropogenic emission estimates for the 30-90°N (a) and 30-90°S (b) latitudinal bands by aggregate sectors (Hoesly et al., 2018): energy, Industry, RCO, and transportation. "RCO" stands for residential, commercial, and other. "Fossil fuel combustion" combines all sectors listed before, and small contributions from the waste and shipping sectors (grouped together). Biomass burning emissions from the 30-90° latitudinal bands are from van Marle et al. (2017).

5.4. Biomass burning emissions in the Southern Hemisphere since preindustrial times

Evolution of biomass burning emission inventories since PI times have been recently subject to debate. Biomass burning emission inventories, such as the CMIP6 inventories, commonly scale up fire emission with population (e.g., van Marle et al., 2017; van der Werf et al., 2013), suggesting lower biomass burning emission in PI compared to present day. On the other side, hypothesizing a decline in burned areas with increasing population density due to land use changes (Andela et al., 2017; Knorr et al., 2014) lead to biomass burning reaching higher levels in the PI compared to present day (e.g., Hamilton et al., 2018; Liu et al., 2021; Rowlinson et al., 2020). Notably, Liu et al. (2021) concluded that fire emissions remained relatively stable in the SH between 1750 and ~1920 CE followed by a 30% decrease until about 1990 CE. These authors support this conclusion by a comparison of simulated black carbon (BC) deposition fluxes with BC measurement conducted on an array of ice cores (14 Antarctica records, and one record from the Andes).

Our SH [CO] reconstruction from ice archives, as well as the recent SH CO record from Strawson et al. (2024), do not show any decreasing trend in [CO] between 1850 and 1992 CE (Fig. 2b). Instead, atmospheric CO in the southern hemisphere exhibits an increase closely reproduced by AerChemMIP models. If the trend in biomass burning

14

inventories used in the frame of CMIP6 (Fig. 4b) were wrong, as suggested by Liu et al. (2021), this would mean that the trend in anthropogenic CO emissions (Fig. 4) would also be wrong (i.e., underestimated), compensating for an overestimation of CO fire emissions. This seems unlikely.

The Antarctic [CO] reconstructions (Strawson et al., 2024; Faïn et al., 2023) also disagree with the elevated [CO] levels reported previously by Wang et al. (2010) which concluded that biomass burning CO emissions peaked during the late 19th century at rates roughly 3 times modern levels (see Faïn et al., 2023, for a detailed comparison with the Wang et al. CO dataset). Finally, both models and observations reveal a [CO] growth rate in the SH a factor of 2 larger during the 1945-1980 CE time period. The modeled trend is mostly driven by an increase in anthropogenic transportation emissions (Fig. 4), and the Antarctica ice archives suggest that such CO anthropogenic emissions are well constrained.

6. Summary and conclusion

We have reported the first bipolar comparison of atmospheric CO mixing ratio extracted from Greenland and Antarctic ice archives with multimodel ACCMIP and AerChemMIP historical ensembles, for the period 1850 to the present. Specifically, the ice archive [CO] records are composites based on multiple ice core and firn air records, respectively 8 and 10 datasets for Greenland and Antarctica (Faïn et al., 2023, 2022; Petrenko et al., 2013). We used historical CO mixing ratio outputs from the 16 ACCMIP models (Naik et al., 2013) for three time slices (1850, 1980, and 2000 CE), and from 7 models involved in the AerChemMIP exercise (Collins et al., 2017) for the historical period spanning 1850-2014 CE at annual resolution.

Both ACCMIP and AerChemMIP model ensembles present negative CO biases at high latitudes, particularly in the northern hemisphere, which are still poorly understood and could involve missing anthropogenic emissions, underestimation of the secondary chemical production of CO, or excessive CO losses via OH oxidation. However, the model CO bias at high northern latitudes has decreased by ~50% between the ACCMIP and AerChemMIP exercises. We used the atmospheric [CO] from Greenland and Antarctica ice archives as a benchmark for ACCMIP and AerChemMIP ensembles to assess both the global chemistry-climate models and the emission datasets they used. Over the period 1980-2010 CE, CO trends from ice archives and AerChemMIP multimodel outputs are in excellent agreement at both northern and southern high latitudes. Such agreement suggests that the trends in surface emissions of CO (including anthropogenic emissions), as well as in the main CO sink (OH oxidation), are now accurately represented within models.

Over the 1920 to 1980 CE, a mismatch in [CO] trends remains between the AerChemMIP multimodel mean and the ice archive dataset in the NH, with the multimodel mean showing lower trend before 1945, and higher trend after 1945. Although Greenland ice archive record should only be considered as an upper bound of the past CO abundance, as we cannot fully rule out in situ production artifacts (Faïn et al., 2022), we suggest that the mismatch between modeled and observed CO trends at high NH latitudes is related to uncertainties in anthropogenic CO emission factors, specifically EF for residential commercial and other, and transportation sectors. Our study indicates that a better evaluation of these EFs would be an area of improvement for modeling of the past NH [CO]. Finally, SH atmospheric [CO] exhibits an increase closely reproduced by AerChemMIP models, supporting the biomass burning inventories

used in the frame of CMIP6 (van Marle et al., 2017). The hypothesis of higher fire emissions at the onset of the 20th century (e.g., Liu et al., 2021) seems unlikely in the light of our results and those of Strawson et al. (2024) who used box-modeling to reconstruct historical fire emissions.

Although imperfect, state of the art global chemistry-climate models now exhibit good capabilities in representing trends in atmospheric [CO] at high latitudes. Further modeling sensitivity studies would provide a better understanding of the nature of the CO bias at high NH latitudes and this study shows that CO trends from ice cores can now serve as a constraint to better disentangle the causes in CO bias. Also, isotopic information can help to determine the various CO sources and their relative magnitudes (e.g., Röckmann et al., 2002). Including isotope data in modeling atmospheric chemistry schemes has been shown to help constraining source strengths of CO (Park et al., 2015). Thus, more measurements of the stable isotopes of CO from firn and ice cores would help constrain relative CO source strengths in the past. This work offers a new constraint to better characterize emissions factors over the past century and thus could contribute to a revision of past tropospheric ozone or methane lifetime evolutions. On the other hand, a recent record from Strawson et al. (2024) suggests that atmospheric SH [CO] may have experienced greater trend variability than predicted for by state-of-the-art chemistry-climate models, suggesting that historical CO dynamics have not been fully accounted for. Improvement in the assessment of past OH trends (e.g., using innovative proxies such as 14CO, Brenninkmeijer et al., 2022) would also provide powerful constraints on the past evolution of the main CO sink.

Competing interests

The contact author has declared that none of the authors has any competing interests.

References

Andela, N., Morton, D. C., Giglio, L., Chen, Y., van der Werf, G. R., Kasibhatla, P. S., DeFries, R. S., Collatz, G. J., Hantson, S., Kloster, S., Bachelet, D., Forrest, M., Lasslop, G., Li, F., Mangeon, S., Melton, J. R., Yue, C., and Randerson, J. T.: A human-driven decline in global burned area, Science, 356, 1356–1362, https://doi.org/10.1126/science.aal4108, 2017.

Archibald, A. T., O'Connor, F. M., Abraham, N. L., Archer-Nicholls, S., Chipperfield, M. P., Dalvi, M., Folberth, G. A., Dennison, F., Dhomse, S. S., Griffiths, P. T., Hardacre, C., Hewitt, A. J., Hill, R. S., Johnson, C. E., Keeble, J., Köhler, M. O., Morgenstern, O., Mulcahy, J. P., Ordóñez, C., Pope, R. J., Rumbold, S. T., Russo, M. R., Savage, N. H., Sellar, A., Stringer, M., Turnock, S. T., Wild, O., and Zeng, G.: Description and evaluation of the UKCA stratosphere–troposphere chemistry scheme (StratTrop vn 1.0) implemented in UKESM1, Geosci. Model Dev., 13, 1223–1266, https://doi.org/10.5194/gmd-13-1223-2020, 2020.

Bauer, S. E., Tsigaridis, K., Faluvegi, G., Kelley, M., Lo, K. K., Miller, R. L., Nazarenko, L., Schmidt, G. A., and Wu, J.: Historical (1850–2014) Aerosol Evolution and Role on Climate Forcing Using the GISS ModelE2.1 Contribution to CMIP6, J. Adv. Model. Earth Syst., 12, e2019MS001978, https://doi.org/10.1029/2019MS001978, 2020.

Brenninkmeijer, C. A. M., Gromov, S. S., and Jöckel, P.: Cosmogenic 14CO for assessing the oh-based self-cleaning capacity of the troposphere, Radiocarbon, 64, 761–779, https://doi.org/10.1017/RDC.2021.101, 2022.

Bruhn, D., Albert, K. R., Mikkelsen, T. N., and Ambus, P.: UV-induced carbon monoxide emission from living vegetation, Biogeosciences, 10, 7877–7882, https://doi.org/10.5194/bg-10-7877-2013, 2013.

Buchholz, R. R., Worden, H. M., Park, M., Francis, G., Deeter, M. N., Edwards, D. P., Emmons, L. K., Gaubert, B., Gille, J., Martínez-Alonso, S., Tang, W., Kumar, R., Drummond, J. R., Clerbaux, C., George, M., Coheur, P.-F., Hurtmans, D., Bowman, K. W., Luo, M., Payne, V. H., Worden, J. R., Chin, M., Levy, R. C., Warner, J., Wei, Z., and Kulawik, S. S.: Air pollution trends measured from Terra: CO and AOD over industrial, fire-prone, and background regions, Remote Sens. Environ., 256, 112275, https://doi.org/10.1016/J.RSE.2020.112275, 2021.

Collins, W. J., Lamarque, J.-F., Schulz, M., Boucher, O., Eyring, V., Hegglin, M. I., Maycock, A., Myhre, G., Prather, M., Shindell, D. T., and Smith, S. J.: AerChemMIP: quantifying the effects of chemistry and aerosols in CMIP6, Geosci. Model Dev., 10, 585–607, https://doi.org/10.5194/gmd-10-585-2017, 2017.

Conte, L., Szopa, S., Séférian, R., and Bopp, L.: The oceanic cycle of carbon monoxide and its emissions to the atmosphere, Biogeosciences, 16, 881–902, https://doi.org/10.5194/bg-16-881-2019, 2019.

Crutzen, P. J.: A discussion of the chemistry of some minor constituents in the stratosphere and troposphere, Pure Appl. Geophys., 106–108, 1385–1399, https://doi.org/10.1007/BF00881092, 1973.

Duncan, B. N., Logan, J. A., Bey, I., Megretskaia, I. A., Yantosca, R. M., Novelli, P. C., Jones, N. B., and Rinsland, C. P.: Global budget of CO, 1988-1997: Source estimates and validation with a global model, J. Geophys. Res.-Atmospheres, 112, D22301, https://doi.org/10.1029/2007jd008459, 2007.

Dunne, J. P., Horowitz, L. W., Adcroft, A. J., Ginoux, P., Held, I. M., John, J. G., Krasting, J. P., Malyshev, S., Naik, V., Paulot, F., Shevliakova, E., Stock, C. A., Zadeh, N., Balaji, V., Blanton, C., Dunne, K. A., Dupuis, C., Durachta, J., Dussin, R., Gauthier, P. P. G., Griffies, S. M., Guo, H., Hallberg, R. W., Harrison, M., He, J., Hurlin, W., McHugh, C., Menzel, R., Milly, P. C. D., Nikonov, S., Paynter, D. J., Ploshay, J., Radhakrishnan, A., Rand, K., Reichl, B. G., Robinson, T., Schwarzkopf, D. M., Sentman, L. T., Underwood, S., Vahlenkamp, H., Winton, M., Wittenberg, A. T., Wyman, B., Zeng, Y., and Zhao, M.: The GFDL Earth System Model Version 4.1 (GFDL-ESM 4.1): Overall Coupled Model Description and Simulation Characteristics, J. Adv. Model. Earth Syst., 12, e2019MS002015, https://doi.org/10.1029/2019MS002015, 2020.

Emmons, L. K., Schwantes, R. H., Orlando, J. J., Tyndall, G., Kinnison, D., Lamarque, J.-F., Marsh, D., Mills, M. J., Tilmes, S., Bardeen, C., Buchholz, R. R., Conley, A., Gettelman, A., Garcia, R., Simpson, I., Blake, D. R., Meinardi, S., and Pétron, G.: The Chemistry Mechanism in the Community Earth System Model Version 2 (CESM2), J. Adv. Model. Earth Syst., 12, e2019MS001882, https://doi.org/10.1029/2019MS001882, 2020.

Faïn, X., Chappellaz, J., Rhodes, R. H., Stowasser, C., Blunier, T., McConnell, J. R., Brook, E. J., Preunkert, S., Legrand, M., Debois, T., and Romanini, D.: High resolution measurements of carbon monoxide along a late Holocene Greenland ice core: evidence for in situ production, Clim. Past, 10, 987–1000, https://doi.org/10.5194/cp-10-987-2014, 2014.

Faïn, X., Rhodes, R. H., Place, P., Petrenko, V. V., Fourteau, K., Chellman, N., Crosier, E., McConnell, J. R., Brook, E. J., Blunier, T., Legrand, M., and Chappellaz, J.: Northern Hemisphere atmospheric history of carbon monoxide since preindustrial times reconstructed from multiple Greenland ice cores, Clim. Past, 18, 631–647, https://doi.org/10.5194/cp-18-631-2022, 2022.

Faïn, X., Etheridge, D. M., Fourteau, K., Martinerie, P., Trudinger, C. M., Rhodes, R. H., Chellman, N. J., Langenfelds, R. L., McConnell, J. R., Curran, M. A. J., Brook, E. J., Blunier, T., Teste, G., Grilli, R., Lemoine, A., Sturges, W. T., Vannière, B., Freitag, J., and Chappellaz, J.: Southern Hemisphere atmospheric history of carbon monoxide over the late Holocene reconstructed from multiple Antarctic ice archives, Clim. Past, 19, 2287–2311, https://doi.org/10.5194/cp-19-2287-2023, 2023.

Feng, L., Smith, S. J., Braun, C., Crippa, M., Gidden, M. J., Hoesly, R. M., Klimont, Z., van Marle, M., van den Berg, M., and van der Werf, G. R.: The generation of gridded emissions data for CMIP6, Geosci. Model Dev., 13, 461–482, https://doi.org/10.5194/gmd-13-461-2020, 2020.

555 Fortems-Cheiney, A., Chevallier, F., Pison, I., Bousquet, P., Saunois, M., Szopa, S., Cressot, C., Kurosu, T. P., Chance, K., and Fried, A.: The formaldehyde budget as seen by a global-scale multi-constraint and multi-species inversion system, Atmospheric Chem. Phys., 12, 6699–6721, https://doi.org/10.5194/acp-12-6699-2012, 2012.

Gaubert, B., Worden, H. M., Arellano, A. F. J., Emmons, L. K., Tilmes, S., Barré, J., Martinez Alonso, S., Vitt, F., Anderson, J. L., Alkemade, F., Houweling, S., and Edwards, D. P.: Chemical feedback from decreasing carbon monoxide emissions, Geophys. Res. Lett., 44, 9985–9995, https://doi.org/10.1002/2017GL074987, 2017.

560 Gaubert, B., Emmons, L. K., Raeder, K., Tilmes, S., Miyazaki, K., Arellano Jr., A. F., Elguindi, N., Granier, C., Tang, W., Barré, J., Worden, H. M., Buchholz, R. R., Edwards, D. P., Franke, P., Anderson, J. L., Saunois, M., Schroeder, J., Woo, J.-H., Simpson, I. J., Blake, D. R., Meinardi, S., Wennberg, P. O., Crounse, J., Teng, A., Kim, M., Dickerson, R. R., He, H., Ren, X., Pusede, S. E., and Diskin, G. S.: Correcting model biases of CO in East Asia: impact on oxidant distributions during KORUS-AQ, Atmospheric Chem. Phys., 20, 14617–14647, https://doi.org/10.5194/acp-20-565 14617-2020, 2020.

Griffiths, P. T., Murray, L. T., Zeng, G., Shin, Y. M., Abraham, N. L., Archibald, A. T., Deushi, M., Emmons, L. K., Galbally, I. E., Hassler, B., Horowitz, L. W., Keeble, J., Liu, J., Moeini, O., Naik, V., O'Connor, F. M., Oshima, N., Tarasick, D., Tilmes, S., Turnock, S. T., Wild, O., Young, P. J., and Zanis, P.: Tropospheric ozone in CMIP6 simulations, Atmospheric Chem. Phys., 21, 4187–4218, https://doi.org/10.5194/acp-21-4187-2021, 2021.

570 Guenther, A., Karl, T., Harley, P., Wiedinmyer, C., Palmer, P. I., and Geron, C.: Estimates of global terrestrial isoprene emissions using MEGAN (Model of Emissions of Gases and Aerosols from Nature), Atmospheric Chem. Phys., 6, 3181–3210, https://doi.org/10.5194/acp-6-3181-2006, 2006.

Haan, D. and Raynaud, D.: Ice core record of CO variations during the last two millennia: atmospheric implications and chemical interactions within the Greenland ice, Tellus Ser. B-Chem. Phys. Meteorol., 50, 253–262, 1998.

575 Haan, D., Martinerie, P., and Raynaud, D.: Ice core data of atmospheric carbon monoxide over Antarctica and Greenland during the last 200 years, Geophys. Res. Lett., 23, 2235–2238, 1996.

Hamilton, D. S., Hantson, S., Scott, C. E., Kaplan, J. O., Pringle, K. J., Nieradzik, L. P., Rap, A., Folberth, G. A., Spracklen, D. V., and Carslaw, K. S.: Reassessment of pre-industrial fire emissions strongly affects anthropogenic aerosol forcing, Nat. Commun., 9, 3182, https://doi.org/10.1038/s41467-018-05592-9, 2018.

580 Hantson, S., Knorr, W., Schurgers, G., Pugh, T. A. M., and Arneth, A.: Global isoprene and monoterpene emissions under changing climate, vegetation, CO2 and land use, Atmos. Environ., 155, 35–45, https://doi.org/10.1016/j.atmosenv.2017.02.010, 2017.

Heimann, I., Griffiths, P. T., Warwick, N. J., Abraham, N. L., Archibald, A. T., and Pyle, J. A.: Methane Emissions in a Chemistry-Climate Model: Feedbacks and Climate Response, J. Adv. Model. Earth Syst., 12, 585 https://doi.org/10.1029/2019MS002019, 2020.

Hoesly, R. M., Smith, S. J., Feng, L., Klimont, Z., Janssens-Maenhout, G., Pitkanen, T., Seibert, J. J., Vu, L., Andres, R. J., Bolt, R. M., Bond, T. C., Dawidowski, L., Kholod, N., Kurokawa, J., Li, M., Liu, L., Lu, Z., Moura, M. C. P., O'Rourke, P. R., and Zhang, Q.: Historical (1750–2014) anthropogenic emissions of reactive gases and aerosols from the Community Emissions Data System (CEDS), Geosci. Model Dev., 11, 369–408, https://doi.org/10.5194/gmd-11-590 369-2018, 2018.

Horowitz, L. W., Naik, V., Paulot, F., Ginoux, P. A., Dunne, J. P., Mao, J., Schnell, J., Chen, X., He, J., John, J. G., Lin, M., Lin, P., Malyshev, S., Paynter, D., Shevliakova, E., and Zhao, M.: The GFDL Global Atmospheric Chemistry-Climate Model AM4.1: Model Description and Simulation Characteristics, J. Adv. Model. Earth Syst., 12, e2019MS002032, https://doi.org/10.1029/2019MS002032, 2020.

595 IPCC, 2023. In: Climate Change 2023: Synthesis Report. Contribution of Working Groups I, II and III to the Sixth Assessment Report of the Intergovernmental Panel on Climate Change [Core Writing Team, H. Lee and J. Romero (eds.)]. IPCC, Geneva, Switzerland, pp. 35-115, doi: 10.59327/IPCC/AR6-978929169164.

Khalil, M. A. K., Pinto, J. P., and Shearer, M. J.: Atmospheric carbon monoxide, Chemosphere - Glob. Change Sci., 1, ix–xi, https://doi.org/10.1016/S1465-9972(99)00053-7, 1999.

600 Knorr, W., Kaminski, T., Arneth, A., and Weber, U.: Impact of human population density on fire frequency at the global scale, Biogeosciences, 11, 1085–1102, https://doi.org/10.5194/bg-11-1085-2014, 2014.

Lamarque, J.-F., Bond, T. C., Eyring, V., Granier, C., Heil, A., Klimont, Z., Lee, D., Liousse, C., Mieville, A., Owen, B., Schultz, M. G., Shindell, D. T., Smith, S. J., Stehfest, E., van Aardenne, J. A., Cooper, O. R., Kainuma, M., Mahowald, N., McConnell, J. R., Naik, V., Riahi, K., and van Vuuren, D. P.: Historical (1850-2000) gridded
605 anthropogenic and biomass burning emissions of reactive gases and aerosols: methodology and application, Atmospheric Chem. Phys., 10, 7017–7039, https://doi.org/10.5194/acp-10-7017-2010, 2010.

Lamarque, J.-F., Shindell, D. T., Josse, B., Young, P. J., Cionni, I., Eyring, V., Bergmann, D., Cameron-Smith, P., Collins, W. J., Doherty, R., Dalsoren, S., Faluvegi, G., Folberth, G., Ghan, S. J., Horowitz, L. W., Lee, Y. H., MacKenzie, I. a., Nagashima, T., Naik, V., Plummer, D., Righi, M., Rumbold, S. T., Schulz, M., Skeie, R. B.,
610 Stevenson, D. S., Strode, S., Sudo, K., Szopa, S., Voulgarakis, a., and Zeng, G.: The Atmospheric Chemistry and Climate Model Intercomparison Project (ACCMIP): overview and description of models, simulations and climate diagnostics, Geosci. Model Dev., 6, 179–206, https://doi.org/10.5194/gmd-6-179-2013, 2013.

Liu, P., Kaplan, J. O., Mickley, L. J., Li, Y., Chellman, N. J., Arienzo, M. M., Kodros, J. K., Pierce, J. R., Sigl, M., Freitag, J., Mulvaney, R., Curran, M. A. J., and McConnell, J. R.: Improved estimates of preindustrial biomass burning
615 reduce the magnitude of aerosol climate forcing in the Southern Hemisphere, Sci. Adv., eabc1379, 2021.

Loh, Z., Langenfelds, R. L., and Krummel, P. B.: Atmospheric CO at Mawson by Commonwealth Scientific and Industrial Research Organisation, CO_MAA_surfaceflask_CSIRO_data1, WDCGG [data set], ver.2021-04-08-1004, https://doi.org/10.50849/WDCGG_0016-7005-3001-01-029999, 2021.

van Marle, M., Kloster, S., Magi, B. I., Marlon, J. R., Daniau, A.-L., Field, R. D., Arneth, A., Forrest, M., Hantson,
620 S., Kehrwald, N. M., Knorr, W., Lasslop, G., Li, F., Mangeon, S., Yue, C., Kaiser, J. W., and van der Werf, G. R.: Historic global biomass burning emissions for CMIP6 (BB4CMIP) based on merging satellite observations with proxies and fire models (1750–2015), Geosci. Model Dev., 10, 3329–3357, https://doi.org/10.5194/gmd-10-3329-2017, 2017.

Meinshausen, M., Vogel, E., Nauels, A., Lorbacher, K., Meinshausen, N., Etheridge, D. M., Fraser, P. J., Montzka, S.
625 A., Rayner, P. J., Trudinger, C. M., Krummel, P. B., Beyerle, U., Canadell, J. G., Daniel, J. S., Enting, I. G., Law, R. M., Lunder, C. R., O'Doherty, S., Prinn, R. G., Reimann, S., Rubino, M., Velders, G. J. M., Vollmer, M. K., Wang,

R. H. J., and Weiss, R.: Historical greenhouse gas concentrations for climate modelling (CMIP6), Geosci. Model Dev., 10, 2057–2116, https://doi.org/10.5194/gmd-10-2057-2017, 2017.

Miyazaki, K., Bowman, K. W., Yumimoto, K., Walker, T., and Sudo, K.: Evaluation of a multi-model, multi-constituent assimilation framework for tropospheric chemical reanalysis, Atmospheric Chem. Phys., 20, 931–967, https://doi.org/10.5194/acp-20-931-2020, 2020.

Naik, V., Voulgarakis, A., Fiore, A. M., Horowitz, L. W., Lamarque, J.-F., Lin, M., Prather, M. J., Young, P. J., Bergmann, D., Cameron-Smith, P. J., Cionni, I., Collins, W. J., Dalsøren, S. B., Doherty, R., Eyring, V., Faluvegi, G., Folberth, G., Josse, B., Lee, Y. H., MacKenzie, I. A., Nagashima, T., van Noije, T. P. C., Plummer, D. A., Righi, M., Rumbold, S. T., Skeie, R., Shindell, D. T., Stevenson, D. S., Strode, S., Sudo, K., Szopa, S., and Zeng, G.: Preindustrial to present-day changes in tropospheric hydroxyl radical and methane lifetime from the Atmospheric Chemistry and Climate Model Intercomparison Project (ACCMIP), Atmospheric Chem. Phys., 13, 5277–5298, https://doi.org/10.5194/acp-13-5277-2013, 2013.

Oshima, N., Yukimoto, S., Deushi, M., Koshiro, T., Kawai, H., Tanaka, T. Y., and Yoshida, K.: Global and Arctic effective radiative forcing of anthropogenic gases and aerosols in MRI-ESM2.0, Prog. Earth Planet Sci., 7, 38, https://doi.org/10.1186/s40645-020-00348-w, 2020.

Pacifico, F., Harrison, S. P., Jones, C. D., Arneth, A., Sitch, S., Weedon, G. P., Barkley, M. P., Palmer, P. I., Serça, D., Potosnak, M., Fu, T.-M., Goldstein, A., Bai, J., and Schurgers, G.: Evaluation of a photosynthesis-based biogenic isoprene emission scheme in JULES and simulation of isoprene emissions under present-day climate conditions, Atmospheric Chem. Phys., 11, 4371–4389, https://doi.org/10.5194/acp-11-4371-2011, 2011.

Park, K., Wang, Z., Emmons, L. K., and Mak, J. E.: Variation of atmospheric CO, δ 13 C, and δ 18 O at high northern latitude during 2004–2009: Observations and model simulations, J. Geophys. Res. Atmospheres, 120, https://doi.org/10.1002/2015JD023191, 2015.

Petrenko, V. V., Martinerie, P., Novelli, P. C., Etheridge, D. M., Levin, I., Wang, Z., Blunier, T., Chappellaz, J., Kaiser, J., Lang, P., Steele, L. P., Hammer, S., Mak, J., Langenfelds, R. L., Schwander, J., Severinghaus, J. P., Witrant, E., Petron, G., Battle, M. O., Forster, G., Sturges, W. T., Lamarque, J.-F., Steffen, K., and White, J. W. C.: A 60 yr record of atmospheric carbon monoxide reconstructed from Greenland firn air, Atmospheric Chem. Phys., 13, 7567–7585, https://doi.org/10.5194/acp-13-7567-2013, 2013.

Petron, G., Crotwell, A. M., Dlugokencky, E. J., Madronich, M., Moglia, E., Neff, D., Thoning, K., Wolter, S., and Mund, J. W.: Atmospheric Carbon Monoxide Dry Air Mole Fractions from the NOAA GML Carbon Cycle Cooperative Global Air Sampling Network, 1988-2022, Version: 2023-08-28, https://doi.org/10.15138/33bv-s284, 2023.

Röckmann, T., Jockel, P., Gros, V., Braunlich, M., Possnert, G., and Brenninkmeijer, C. A. M.: Using 14C, 13C, 18O and 17O isotopic variations to provide insights into the high northern latitude surface CO inventory, Atmospheric Chem. Phys., 2, 147–159, 2002.

Rowlinson, M. J., Rap, A., Hamilton, D. S., Pope, R. J., Hantson, S., Arnold, S. R., Kaplan, J. O., Arneth, A., Chipperfield, M. P., Forster, P. M., and Nieradzik, L.: Tropospheric ozone radiative forcing uncertainty due to pre-

industrial fire and biogenic emissions, Atmospheric Chem. Phys., 20, 10937–10951, https://doi.org/10.5194/acp-20-10937-2020, 2020.

665 Rubino, M., Etheridge, D. M., Thornton, D. P., Howden, R., Allison, C. E., Francey, R. J., Langenfelds, R. L., Steele, L. P., Trudinger, C. M., Spencer, D. A., Curran, M. A. J., van Ommen, T. D., and Smith, A. M.: Revised records of atmospheric trace gases CO2,CH4,N2O, and d13CO2 over the last 2000 years from Law Dome, Antarctica, Earth Syst. Sci. Data, 11, 473–492, https://doi.org/10.5194/essd-11-473-2019, 2019.

Schultz, M. G., Akimoto, H., Bottenheim, J., Buchmann, B., Galbally, I. E., Gilge, S., Helmig, D., Koide, H., Lewis,
670 A. C., Novelli, P. C., Plass-Dölmer, C., Ryerson, T. B., Steinbacher, M., Steinbrecher, R., Tarasova, O., Tørseth, K., Thouret, V., and Zellweger, C.: The global atmosphere watch reactive gases measurement network, Elementa, 3, 1–23, https://doi.org/10.12952/journal.elementa.000067, 2015.

Shindell, D. T., Faluvegi, G., Stevenson, D. S., Krol, M. C., Emmons, L. K., Lamarque, J.-F., Pétron, G., Dentener, F. J., Ellingsen, K., Schultz, M. G., Wild, O., Amann, M., Atherton, C. S., Bergmann, D. J., Bey, I., Butler, T., Cofala,
675 J., Collins, W. J., Derwent, R. G., Doherty, R. M., Drevet, J., Eskes, H. J., Fiore, A. M., Gauss, M., Hauglustaine, D. A., Horowitz, L. W., Isaksen, I. S. A., Lawrence, M. G., Montanaro, V., Müller, J.-F., Pitari, G., Prather, M. J., Pyle, J. A., Rast, S., Rodriguez, J. M., Sanderson, M. G., Savage, N. H., Strahan, S. E., Sudo, K., Szopa, S., Unger, N., van Noije, T. P. C., and Zeng, G.: Multimodel simulations of carbon monoxide: Comparison with observations and projected near-future changes, J. Geophys. Res., 111, D19306, https://doi.org/10.1029/2006JD007100, 2006.

680 Stein, O., Schultz, M. G., Bouarar, I., Clark, H., Huijnen, V., Gaudel, A., George, M., and Clerbaux, C.: On the wintertime low bias of Northern Hemisphere carbon monoxide found in global model simulations, Atmospheric Chem. Phys., 14, 9295–9316, https://doi.org/10.5194/acp-14-9295-2014, 2014.

Stevenson, D. S., Zhao, A., Naik, V., O'Connor, F. M., Tilmes, S., Zeng, G., Murray, L. T., Collins, W. J., Griffiths, P. T., Shim, S., Horowitz, L. W., Sentman, L. T., and Emmons, L. K.: Trends in global tropospheric hydroxyl radical
685 and methane lifetime since 1850 from AerChemMIP, Atmospheric Chem. Phys., 20, 12905–12920, https://doi.org/10.5194/acp-20-12905-2020, 2020.

Strawson, I., Faïn, X., Bauska, T. K., Muschitiello, F., Vladimirova, D. O., Tetzner, D. R., Humby, J., Thomas, E. R., Liu, P., Zhang, B., Grilli, R., and Rhodes, R. H.: Historical Southern Hemisphere biomass burning variability inferred from ice core carbon monoxide records, Proc. Natl. Acad. Sci. U.S.A., 121, e2402868121,
690 https://doi.org/10.1073/pnas.2402868121, 2024.

Strode, S. A., Duncan, B. N., Yegorova, E. A., Kouatchou, J., Ziemke, J. R., and Douglass, A. R.: Implications of carbon monoxide bias for methane lifetime and atmospheric composition in chemistry climate models, Atmospheric Chem. Phys., 15, 11789–11805, https://doi.org/10.5194/acp-15-11789-2015, 2015.

Szopa, S., Naïk, V., Adhikary, B., Artaxo, P., Berntsen, T., Collins, W. D., Fuzzi, S., Gallardo, L., Kiendler-Scharr,
695 A., Klimont, Z., Liao, H., Unger, N., and Zanis, P.: Climate Change 2021 – The Physical Science Basis. Contribution of Working Group I to the Sixth Assessment Report of the Intergovernmental Panel on Climate Change [Masson-Delmotte, V., P. Zhai, A. Pirani, S.L. Connors, C. Péan, S. Berger, N. Caud, Y. Chen, L. Goldfarb, M.I. Gomis, M. Huang, K. Leitzell, E. Lonnoy, J.B.R. Matthews, T.K. Maycock, T. Waterfield, O. Yelekçi, R. Yu, and B. Zhou (eds.)],

1st ed., Cambridge University Press, Cambridge, United Kingdom and New York, NY, USA, pp. 817–922, https://doi.org/10.1017/9781009157896.008, 2021.

Wang, Z., Chappellaz, J., Park, J. Y., and Mak, J.: Large variations in Southern Hemisphere biomass burning during the last 650 years, Science, 330, 1663–166, https://doi.org/10.1126/science.1197257, 2010.

Wang, Z., Chappellaz, J., Martinerie, P., Park, K., Petrenko, V. V., Witrant, E., Emmons, L. K., Blunier, T., Brenninkmeijer, C. A. M., and Mak, J.: The isotopic record of Northern Hemisphere atmospheric carbon monoxide since 1950: implications for the CO budget, Atmospheric Chem. Phys., 12, 4365–4377, https://doi.org/10.5194/acp-12-4365-2012, 2012.

van der Werf, G. R., Peters, W., van Leeuwen, T. T., and Giglio, L.: What could have caused pre-industrial biomass burning emissions to exceed current rates?, Clim. Past, 9, 289–306, https://doi.org/10.5194/cp-9-289-2013, 2013.

van der Werf, G. R., Randerson, J. T., Giglio, L., van Leeuwen, T. T., Chen, Y., Rogers, B. M., Mu, M., van Marle, M., Morton, D. C., Collatz, G. J., Yokelson, R. J., and Kasibhatla, P. S.: Global fire emissions estimates during 1997–2016, Earth Syst. Sci. Data, 9, 697–720, https://doi.org/10.5194/essd-9-697-2017, 2017.

Van Noije, T., Bergman, T., Le Sager, P., O'Donnell, D., Makkonen, R., Gonçalves-Ageitos, M., Döscher, R., Fladrich, U., Von Hardenberg, J., Keskinen, J.-P., Korhonen, H., Laakso, A., Myriokefalitakis, S., Ollinaho, P., Pérez García-Pando, C., Reerink, T., Schrödner, R., Wyser, K., and Yang, S.: EC-Earth3-AerChem: a global climate model with interactive aerosols and atmospheric chemistry participating in CMIP6, Geosci. Model Dev., 14, 5637–5668, https://doi.org/10.5194/gmd-14-5637-2021, 2021.

Wild, O., Voulgarakis, A., O'Connor, F., Lamarque, J.-F., Ryan, E. M., and Lee, L.: Global sensitivity analysis of chemistry–climate model budgets of tropospheric ozone and OH: exploring model diversity, Atmospheric Chem. Phys., 20, 4047–4058, https://doi.org/10.5194/acp-20-4047-2020, 2020.

Winijkul, E., Fierce, L., and Bond, T. C.: Emissions from residential combustion considering end-uses and spatial constraints: Part I, methods and spatial distribution, Atmos. Environ., 125, 126–139, https://doi.org/10.1016/j.atmosenv.2015.10.013, 2016.

Wu, T., Zhang, F., Zhang, J., Jie, W., Zhang, Y., Wu, F., Li, L., Yan, J., Liu, X., Lu, X., Tan, H., Zhang, L., Wang, J., and Hu, A.: Beijing Climate Center Earth System Model version 1 (BCC-ESM1): model description and evaluation of aerosol simulations, Geoscientific Model Development, 13, 977–1005, https://doi.org/10.5194/gmd-13-977-2020, 2020.

Young, P. J., Archibald, A. T., Bowman, K. W., Lamarque, J.-F., Naik, V., Stevenson, D. S., Tilmes, S., Voulgarakis, A., Wild, O., Bergmann, D., Cameron-Smith, P., Cionni, I., Collins, W. J., Dalsøren, S. B., Doherty, R. M., Eyring, V., Faluvegi, G., Horowitz, L. W., Josse, B., Lee, Y. H., MacKenzie, I. A., Nagashima, T., Plummer, D. A., Righi, M., Rumbold, S. T., Skeie, R. B., Shindell, D. T., Strode, S. A., Sudo, K., Szopa, S., and Zeng, G.: Pre-industrial to end 21st century projections of tropospheric ozone from the Atmospheric Chemistry and Climate Model Intercomparison Project (ACCMIP), Atmospheric Chemistry and Physics, 13, 2063–2090, https://doi.org/10.5194/acp-13-2063-2013, 2013.

Yukimoto, S., Kawai, H., Koshiro, T., Oshima, N., Yoshida, K., Urakawa, S., Tsujino, H., Deushi, M., Tanaka, T., Hosaka, M., Yabu, S., Yoshimura, H., Shindo, E., Mizuta, R., Obata, A., Adachi, Y., and Ishii, M.: The meteorological

research institute Earth system model version 2.0, MRI-ESM2.0: Description and basic evaluation of the physical component, J. Meteorol. Soc. Jpn., 97, 931–965, https://doi.org/10.2151/jmsj.2019-051, 2019.

Zhang, J., Wu, T., Zhang, F., Furtado, K., Xin, X., Shi, X., Li, J., Chu, M., Zhang, L., Liu, Q., Yan, J., Wei, M., and Ma, Q.: BCC-ESM1 Model Datasets for the CMIP6 Aerosol Chemistry Model Intercomparison Project

740   (AerChemMIP), Adv. Atmospheric Sci., 38, 317–328, https://doi.org/10.1007/s00376-020-0151-2, 2021.

Zhao, Y., Saunois, M., Bousquet, P., Lin, X., Berchet, A., Hegglin, M. I., Canadell, J. G., Jackson, R. B., Hauglustaine, D. A., Szopa, S., Stavert, A. R., Abraham, N. L., Archibald, A. T., Bekki, S., Deushi, M., Jöckel, P., Josse, B., Kinnison, D., Kirner, O., Marécal, V., O'Connor, F. M., Plummer, D. A., Revell, L. E., Rozanov, E., Stenke, A., Strode, S., Tilmes, S., Dlugokencky, E. J., and Zheng, B.: Inter-model comparison of global hydroxyl radical (OH)

745   distributions and their impact on atmospheric methane over the 2000–2016 period, Atmos. Chem. Phys., 19, 13701–13723, https://doi.org/10.5194/acp-19-13701-2019, 2019.

Zheng, B., Chevallier, F., Yin, Y., Ciais, P., Fortems-Cheiney, A., Deeter, M. N., Parker, R. J., Wang, Y., Worden, H. M., and Zhao, Y.: Global atmospheric carbon monoxide budget 2000–2017 inferred from multi-species atmospheric inversions, Earth Syst. Sci. Data, 11, 1411–1436, https://doi.org/10.5194/essd-11-1411-2019, 2019.

750